Earth and Planetary Science Letters 307 (2011) 253–265

Contents lists available at ScienceDirect

Earth and Planetary Science Letters

journal homepage: www.elsevier.com/locate/epsl

Iron fertilisation and biogeochemical cycles in the sub-Arctic northwest Pacific during the late Pliocene intensification of northern hemisphere glaciation

Ian Bailey [a,*,1], Qingsong Liu [b,1], George E.A. Swann [c], Zhaoxia Jiang [b], Youbin Sun [d], Xiang Zhao [a], Andrew P. Roberts [a,2]

[a] School of Ocean and Earth Science, National Oceanography Centre, University of Southampton, European Way, Southampton SO14 3ZH, UK
[b] Paleomagnetism and Geochronology Laboratory (SKL-LE), Institute of Geology and Geophysics, Chinese Academy of Sciences, Beijing 100029, People's Republic of China
[c] School of Geography, University of Nottingham, University Park, Nottingham, NG7 2RD, UK
[d] State Key Laboratory of Loess and Quaternary Geology, Institute of Earth Environment, Chinese Academy of Sciences, Xi'an 710075, People's Republic of China

ARTICLE INFO

Article history:
Accepted 17 May 2011
Available online 2 June 2011

Editor: P. DeMenocal

Keywords:
aeolian dust
volcanic glass
ice rafted debris
North Pacific
nutrient use
northern hemisphere glaciation

ABSTRACT

Increases in the low-field mass-specific magnetic susceptibility (χ), dropstones and the terrigenous sediment component from Ocean Drilling Program (ODP) Site 882 (~45°N) have been interpreted to indicate a major onset of ice-rafting to the sub-Arctic northwest Pacific Ocean during marine isotope stage (MIS) G6 (from ~2.75 Ma). In contrast, studies of the terrigenous content of sediments cored downwind of ODP Site 882 indicate that dust and disseminated volcanic ash deposition in the sub-Arctic Pacific increased markedly during MIS G6. To investigate the relative contribution of dust, volcanic ash and ice rafting to the Pliocene χ increase, we present new high-resolution environmental magnetic and ice-rafted debris records from ODP Sites 882 and 885. Our results demonstrate that the χ increase at both sites across MIS G6 is predominantly controlled by a previously overlooked mixture of aeolian dust and volcanic ash. Our findings call into question the reliability of χ as a proxy for ice-rafting to the North Pacific. They also highlight a previously undocumented link between iron fertilisation and biogeochemical cycling in the North Pacific at a key stage during intensification of late Pliocene northern hemisphere glaciation.

1. Introduction

The modern sub-Arctic Pacific Ocean is characterised by a permanent halocline that reduces exchange between its surface and deep-waters, which results in a large annual range (~11 °C) in sea-surface temperature (Haug et al., 2005). Halocline development during the late Pliocene (at ~2.73 Ma, during marine isotope stage (MIS) G6) (Haug et al., 1999, 2005), when abundant northern hemisphere-wide iceberg rafting is documented (Kleiven et al., 2002; Maslin et al., 1998), has led to the suggestion that enhanced seasonal surface warming of the sub-Arctic Pacific Ocean provided the vapour that fuelled large-scale glaciation of North America (Haug et al., 2005). The resultant isolation of CO_2-rich North Pacific deep-waters may also have played an important role in buffering the decline in atmospheric pCO_2 that began some ~450 ka earlier (from ~3.2 Ma) (Seki et al., 2010) and in setting the baseline state for subsequent Plio-Pleistocene glaciations (Bailey et al., 2010; Lawrence et al., 2009).

Central to the argument for late Pliocene stratification of the sub-Arctic Pacific Ocean is that an abrupt decrease in opal burial at Ocean Drilling Program (ODP) Site 882 (Fig. 1) from 2.73 Ma (Haug et al., 1995) reflects a reduction in upwelling of nutrient-rich deep-waters due to halocline development (Haug et al., 1999). Ratios of ^{30}Si to ^{28}Si ($\delta^{30}Si$) in diatom frustules ($\delta^{30}Si_{diatom}$) and ^{15}N to ^{14}N ($\delta^{15}N$) in bulk sediments ($\delta^{15}N_{bulk}$) can be used to test the stratification hypothesis because they can shed light on changes in nutrient use in, and supply to, the photic zone associated with halocline development. $\delta^{15}N_{bulk}$ data from Site 882 support the contention that the opal drop at 2.73 Ma was due to halocline stratification because they indicate more complete consumption of a smaller pool of surface nitrate by phytoplankton after 2.73 Ma (Sigman et al., 2004). However, contemporaneous diatom $\delta^{30}Si_{diatom}$ data have an opposite trend (Reynolds et al., 2008), which is puzzling because any reduced gross nutrient supply to surface waters should have increased silicic acid consumption.

With a halocline limiting sub-surface upwelling of nutrients, the anti-phase relationship between Site 882 $\delta^{30}Si_{diatom}$ and $\delta^{15}N_{bulk}$ from ~2.73 Ma has been attributed to increased Si:N of nutrients supplied to the photic zone and/or to a change in $\delta^{30}Si$ of silicic acid (Reynolds et al., 2008). However, in Southern Ocean records, bulk sediment and diatom-bound organic matter $\delta^{15}N$ maxima (Crosta and Shemesh, 2002; Schneider-Mor et al., 2005; Sigman et al., 1999) and $\delta^{30}Si_{diatom}$ minima (Brzezinski et al., 2002; De La Rocha et al., 1998) during late Pleistocene

* Corresponding author.
E-mail address: Ian.Bailey@noc.soton.ac.uk (I. Bailey).
[1] These authors contributed equally to this work.
[2] Now at: Research School of Earth Sciences, The Australian National University, Canberra, ACT 0200, Australia.

0012-821X/$ – see front matter © 2011 Elsevier B.V. All rights reserved.
doi:10.1016/j.epsl.2011.05.029

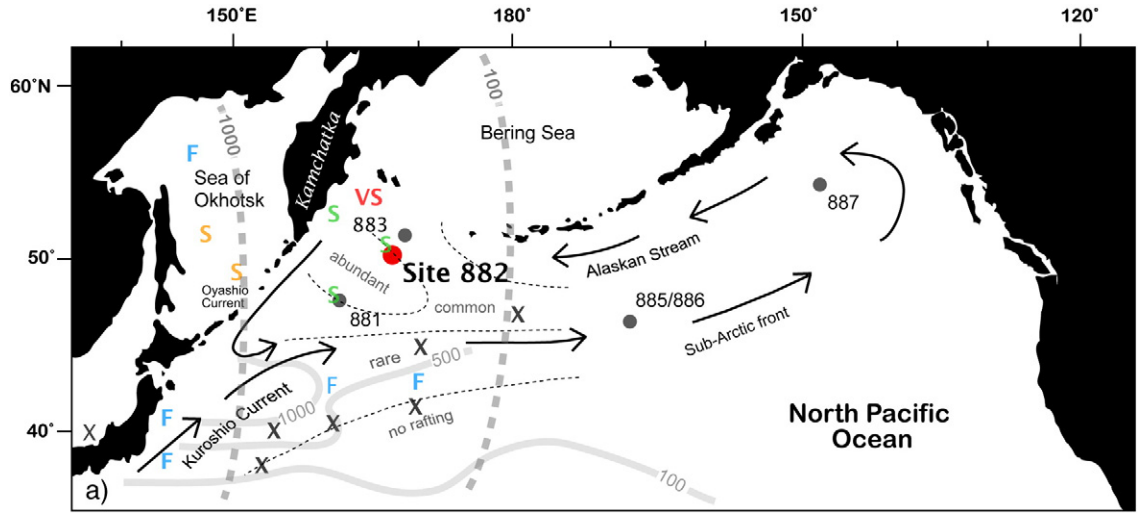

Fig. 1. Location of (a) ODP sites 882 (red circle), 885 and other sub-Arctic North Pacific sites (grey circles) referred to in the text. Arrows denote simplified surface current systems (modified from McKelvey et al. (1995)). Also shown are maps of estimated relative abundance (Conolly and Ewing, 1970) and mass accumulation (Bigg et al., 2008) of North Pacific Last Glacial Maximum coarse lithic ice-rafted debris (IRD). 'X' indicates no evidence of IRD, blue 'F' denotes estimated concentrations <50 mg cm^{-2} ka^{-1}, yellow 'S' ~50–250 mg cm^{-2} ka^{-1}, green 'S' ~250–1000 mg cm^{-2} ka^{-1} and red 'VS' >1000 mg cm^{-2} ka^{-1} in the >63 μm to <2 mm lithogenic fraction. The thick, dashed, grey lines depict contoured estimates of the rate of deposition of mineral aerosol (in mg cm^{-2} ka^{-1}), based on atmospheric transport (Duce et al., 1991) and the solid, thick, light-grey lines represent latest Quaternary mass accumulation rates of dust (in mg cm^{-2} ka^{-1}), based typically on uppermost Quaternary samples and occasionally on an average of Holocene rates (Rea, 1994).

glaciations are often attributed to enhanced dust inputs (Brzezinski et al., 2002). This hypothesis has developed because dust supplies bioavailable Fe (Iwamoto et al., 2011) to surface waters, which lowers diatom frustule Si:N uptake ratios that result in more rapid nitrate (NO_3^-) depletion in the euphotic zone relative to silicic acid ($Si(OH)_4$) (Frank et al., 2000; Hutchins and Bruland, 1998; Matsumoto et al., 2002; Matsumoto and Sarmiento, 2008; Takeda, 1998), although not all studies find such a change (e.g., Hoffmann et al., 2007). A similar chain of events may also arise from enhanced delivery of Fe-rich volcanic ash (Duggen et al., 2010; Hamme et al., 2010).

Records of terrigenous inputs to the North Pacific Ocean indicate that the onset of halocline stratification during MIS G6 is broadly coincident with a marked intensification of dust delivery (Janecek and Rea, 1983; Rea et al., 1998; Sun et al., 2006; Sun and Liu, 2007). At Site 882, terrigenous inputs increase significantly during MIS G6 (Haug et al., 1995). However, understanding the relative importance of aeolian dust to terrigenous inputs at Site 882 and its relationship to biogeochemical cycles is not straightforward because ice-rafting and explosive volcanism provided important additional terrigenous sources during intensification of northern hemisphere glaciation (iNHG) (Pettke et al., 2000; Prueher and Rea, 2001).

Magnetic properties of marine sediments are often highly sensitive to subtle mineralogical and grain size changes that make them useful for determining the origin of terrigenous sediments (Evans and Heller, 2003; Maher and Thompson, 1999; Verosub and Roberts, 1995). The magnetic mineral components of both aeolian dust (Bloemendal and deMenocal, 1989; Clemens and Prell, 1991; deMenocal et al., 1991; Doh et al., 1988; Larrasoaña et al., 2003, 2008; Yamazaki and Ioka, 1997) and ice-rafted debris (IRD) (Grousset et al., 1993; Hall and King, 1989; Robinson et al., 1995; Stoner et al., 1996) often have distinctive magnetic signatures, which makes environmental magnetism useful for investigating palaeoclimatic and palaeoceanographic change.

Increases in low-field mass-specific magnetic susceptibility (χ) and the >2 μm siliciclastic sediment component from Site 882 (~45°N) have been suggested to indicate a major onset of ice-rafting to the sub-Arctic northwest Pacific Ocean during MIS G6 (Haug et al., 1995; Maslin et al., 1995). Whilst sand-sized IRD is found in sub-Arctic northwest Pacific sediments along the sub-Arctic front at ~47–48°N (Conolly and Ewing, 1970; Kent et al., 1971; Krissek, 1995; McKelvey et al., 1995), the abundance of drop stones (Shipboard Scientific Party, 1993) and sand-sized IRD (Conolly and Ewing, 1970; Krissek, 1995) reported from further north are notably low. We therefore cannot be certain whether the magnetic particles responsible for the χ increase at Site 882 at ~2.75 Ma were derived from volcanism, iceberg melting or from dust deposition sourced from Asia. To test between these possibilities, and to improve our understanding of the processes responsible for changes in nutrient use proxies at Site 882 during iNHG, we present new high-resolution environmental magnetic and IRD records from ODP Sites 882 and 885.

2. Background

ODP Site 885 lies at the northern edge of the central North Pacific gyre (44°41′N, 168°16′E; water depth = 5799 m, Fig. 1). This region is characterised by slow Plio-Pleistocene sedimentation (<1 cm ka^{-1}) because of low biological productivity and low terrigenous sediment input. Biogenic silica dominates biogenic sedimentation, whilst Site 885 is sufficiently far south that there is no significant IRD component (Snoeckx et al., 1995). The dominant sediment input is therefore aeolian dust from Asia (Doh et al., 1988; Rea and Janecek, 1981; Snoeckx et al., 1995) and volcanic ash from the Kamchatka–Kurile and Aleutian Arcs (Pettke et al., 2000).

ODP Site 882 is located in the sub-Arctic northwest Pacific (50°22′N, 167°36′E; water depth = 3244 m, Fig. 1), which experienced rapid sedimentation (~10–20 cm ka^{-1}) during the early to mid Pliocene due to high productivity (mostly biogenic silica (Haug et al., 1995; 1999)) and significant terrigenous input. Although terrigenous inputs increased after ~2.75 Ma (from ~0.2 to 0.5 g cm^{-2} ka^{-1}), overall sedimentation rates decreased (to ≤4 cm ka^{-1}), as is observed throughout the sub-Arctic Pacific (Rea et al., 1993) in response to a major drop in productivity following halocline development (Haug et al., 1999; Swann et al., 2006). Whilst Site 882 would have received a significant supply of aeolian dust throughout the Plio-Pleistocene (estimates of modern dust flux to this region are >500 mg cm^{-2} ka^{-1}; Fig. 1) (Duce et al., 1991; Rea, 1994), it is sufficiently far north and proximal to the Kamchatka–Kurile and Aleutian Arcs that melting icebergs derived from east Asia (Maslin et al., 1998) and explosive volcanism (Prueher and

Rea, 2001) provided additional important terrigenous sources of sediment during late Pliocene iNHG.

Although previous environmental magnetic studies of central North Pacific Ocean sediments (south of 30°N) provide important insights into late Pliocene variations in Asian aeolian dust inputs (Doh et al., 1988; Yamazaki and Ioka, 1997), few have focused on the contribution of dust to coeval sub-Arctic Pacific sediments. Although an environmental magnetic study has been undertaken for ODP Site 885 (Arnold et al., 1995), it focused on long time intervals at low resolution (over 0.75 m intervals). Similarly, previous studies of late Pliocene ice rafting to the sub-Arctic Pacific (Krissek, 1995), including to Site 882 (Prueher and Rea, 2001), are not of sufficient resolution to assess controls on terrigenous inputs to Site 882. Thus, to understand the relative contribution of aeolian dust, volcanic ash and IRD to late Pliocene sub-Arctic northwest Pacific χ, high-resolution environmental magnetic and IRD records are reported here.

3. Methods

To facilitate environmental magnetic measurements, u-channel samples (Weeks et al., 1993) were taken from the centre of split cores (core sections 2 H–1 W through 2 H–6 W) from ODP Hole 885A between depths of 4.6 and 13.1 mbsf (metres below sea floor). Discrete samples (8 cm^3, n = 499) were also taken at 1-cm stratigraphic intervals (every ~2.3 ka). Discrete samples (10 cm^3, n = 190) were also taken from ODP Hole 882A (core sections 9 H–1 W through 12 H–4 W) between depths of 75.62 and 109.7 mbsf, at 10 to 30 cm stratigraphic intervals (average every ~5 ka).

3.1. Magnetic measurements

U-channels and discrete samples were analysed using a narrow-access high-resolution 2-G Enterprises cryogenic magnetometre (Weeks et al., 1993) housed within a magnetically shielded laboratory. An anhysteretic remanent magnetization (ARM) was imparted to all samples in a 150 mT alternating field (AF) with a superimposed 50 μT direct bias field. A saturation isothermal remanent magnetization (*SIRM*) was then imparted in a 0.9 T saturation field. The 'hard' isothermal remanent magnetization ($HIRM = 0.5*(-IRM_{-300\ mT} + SIRM)$) was also determined following King and Channell (1991), where $IRM_{-300\ mT}$ is the remanent magnetization obtained after first saturating the sample in a 0.9 T field and then applying a backfield of 300 mT. Generally, high *HIRM* values indicate increased concentrations of hematite and goethite, which are common in aeolian dust. The *S*-ratio ($-IRM_{-300\ mT}/SIRM$) was calculated to determine the relative contributions of low (e.g., magnetite) and high coercivity (e.g., hematite) magnetic minerals. Generally, a low *S*-ratio (<1) indicates significant amounts of high coercivity minerals. An alternative measure of high coercivity magnetic mineral content is the remanence measured after AF demagnetization of an *SIRM* ($SIRM_{AF@X\ mT}$), where *X* indicates the peak AF of *X* mT (Larrasoaña et al., 2003).

The discrete samples were used to determine the room-temperature frequency-dependence of χ at dual frequencies (470 and 4700 Hz), using a Bartington Instruments MS2B magnetic susceptibility metre. The absolute frequency-dependent susceptibility ($\chi_{fd} = \chi_{470\ Hz} - \chi_{4700\ Hz}$) enables quantification of contributions from ultra-fine superparamagnetic (SP) particles (Mullins and Tite, 1973; Stephenson, 1971). To characterise magnetic mineralogy, the temperature dependent susceptibility (χ–T) was measured for representative samples across ~2.75 Ma using a Kappabridge KLY-3 magnetic susceptibility metre, equipped with a CS-3 furnace, from room temperature to 700 °C in an argon environment (with an Ar flux of 50 ml min^{-1}).

Magnetic grains in marine sediment derived from dust deposition reside in the fine sediment fraction (<8 μm (Sun et al., 2004)). Those sourced from melting icebergs will be present as discrete clay and as fine-silt sized particles, but will also be embedded in coarser silt and sand-sized rock grains (Hemming, 2004; Robinson et al., 1995). To examine which size fraction(s) contribute most to the bulk sediment χ, 23 samples containing abundant (or sparse) coarse lithics were divided into four size-fractions on the basis of Stokes' law: <8, 8–16, 16–64, and >64 μm. χ was measured for the four size fractions.

3.2. Lithic grain counts

To examine the history of ice rafting at Site 882, we performed IRD counts of coarse lithic grains (>150 μm) per gramme of dry sediment following Peck et al. (2007). The siliciclastic sediment fraction at Site 882 contains abundant disseminated fresh volcanic detritus (Prueher and Rea, 2001). This is sourced from explosive volcanism along the Kamchatka–Kurile and Aleutian arcs, where volcanic activity intensified during iNHG (Prueher and Rea, 2001). Our counts reveal variable inputs of coarse fresh volcanic glass. Several peaks in volcanic glass (n = 9) correspond to ash layers (Rea et al., 1993). The generally smaller, but variable, numbers of disseminated fresh volcanic glass grains likely originate from explosive volcanism. Nevertheless, because ash may have been sourced from atmospheric fallout or via ice rafting, after fallout onto icebergs, we report IRD counts as both lithics per gramme and lithics minus fresh volcanics per gramme of dry sediment.

3.3. Diatom silicon isotope ($\delta^{30}Si_{diatom}$) measurements

To investigate the relationship between Fe inputs and the biological pump across ~2.73 Ma we made $\delta^{30}Si_{diatom}$ measurements (n = 30) for the interval ~2.85–2.55 Ma at ODP Site 882 in addition to those of Reynolds et al. (2008). Diatoms were extracted using existing techniques with analysed (75–150 μm) fractions dominated by two taxa; *Coscinodiscus marginatus* (Ehrenb.) and *C. radiatus* (Ehrenb.) (Swann, 2010). $\delta^{30}Si_{diatom}$ was analysed using step-wise fluorination at the NERC Isotope Geosciences Laboratory, U.K., with silicon collected as SiF_4. Measurements were made on a Finnigan MAT 253 stable isotope ratio mass spectrometre with values corrected using NIGL within-run laboratory diatom standard BFC_{mod} against NBS28 (Leng and Sloane, 2008). Accuracy is confirmed from inter-laboratory comparisons (Reynolds et al., 2007) (replicate analyses give an analytical reproducibility (1σ) of 0.06‰).

3.4. Age models

The chronology used is based on the magnetic reversal stratigraphy for Site 885A (Dickens et al., 1995; Rea et al., 1993) and on astronomical calibration of the magnetic reversal stratigraphy for Site 882A (Weeks et al., 1995) using physical property data (Tiedemann and Haug, 1995). Our records are from single holes at the respective drill sites and therefore contain a number of stratigraphic gaps between cores. However, the stratigraphic gaps do not prevent us from establishing the dominant source of late Pliocene terrigenous inputs to Site 882.

4. Results and discussion

4.1. Environmental magnetic records for ODP Site 885

The χ increase of sub-Arctic Pacific sediment at ~2.75 Ma is recorded at Site 885 at ~12.6 mbsf (Fig. 2a). χ–T curves for representative samples from Site 885 (Fig. 3b–e) indicate that the dominant magnetic particles responsible for the χ signal are magnetite and low-Ti titanomagnetites, and that magnetic mineralogy did not significantly change across ~2.75 Ma. When magnetic mineralogy remains constant, *ARM*/*SIRM* variability reflects relative changes in magnetic grain size (Thompson and Oldfield, 1986). However, at Site 885, *ARM*/*SIRM* does not change significantly from 12.6 to 12 mbsf when χ increases (Fig. 2c), which indicates that the χ increase at ~2.75 Ma is associated with a change in

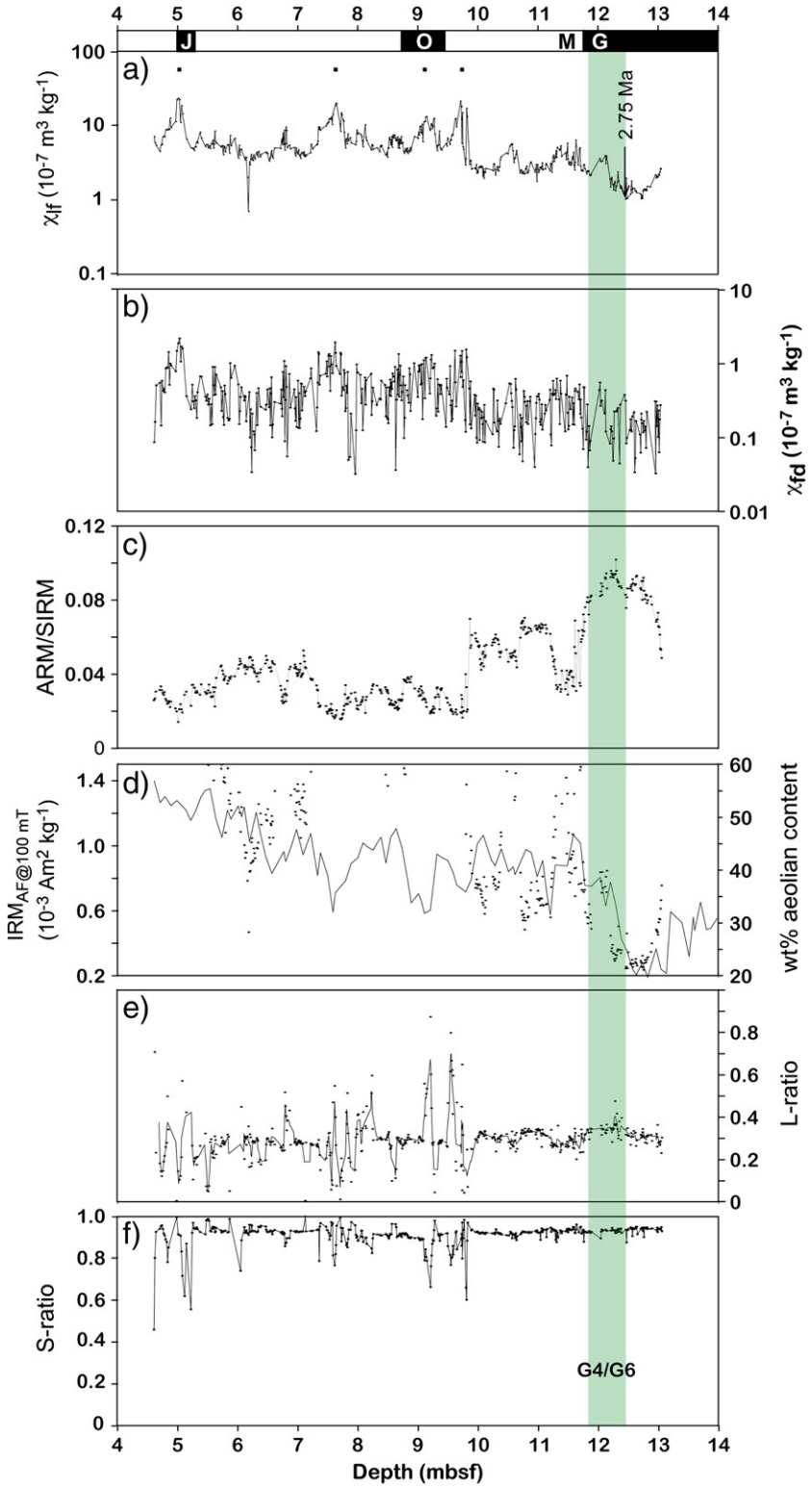

Fig. 2. Plio-Pleistocene magnetic properties of marine sediments from ODP Hole 885A versus depth (in metres below sea floor (mbsf)). (a) Low-field mass-specific magnetic susceptibility, χ, (b) frequency-dependent magnetic susceptibility, χ_{fd}, (c) ARM/SIRM, (d) aeolian dust content (wt.% of bulk sediment, thin black line determined using the method of Sun and Liu (2007)) plotted alongside $IRM_{AF@100\ mT}$ (black dots), (e) *L*-ratio, and (f) *S*-ratio. The *ARM*/*SIRM* ratio can be used to determine relative grain size variations in magnetic minerals. Stable single domain (SD) particles have higher *ARM*, but lower *SIRM*, than coarser particles, so an increase in *ARM*/*SIRM* is taken to indicate a fining of magnetic mineral grain size. The vertical green bar indicates the Plio-Pleistocene palaeoclimatic transition across 2.75 Ma (vertical arrow at ~12.6 mbsf). Label G4/G6 = marine isotope stages G4/G6. The black/white bar at the top of the figure denotes the positions of palaeomagnetic reversal boundaries (Dickens et al., 1995; Rea et al., 1993): base of Jaramillo Subchron = 5.34 mbsf; base of Olduvai Subchron = 9.44 mbsf; Gauss/Matuyama boundary = 11.75 mbsf. χ_{lf} and χ_{fd} data are plotted on a logarithmic scale. Black squares in (a) represent the midpoint depth of discrete burrowed volcanic ash identified in this study from shipboard core images (Rea et al., 1993). Aeolian dust content was estimated after removal of carbonate, organic matter, iron oxides and biogenic opal following the method developed by Rea and Janecek (1981) and Snoeckx et al. (1995). Note that this method cannot differentiate between aeolian dust and disseminated volcanic ash (Pettke et al., 2000).

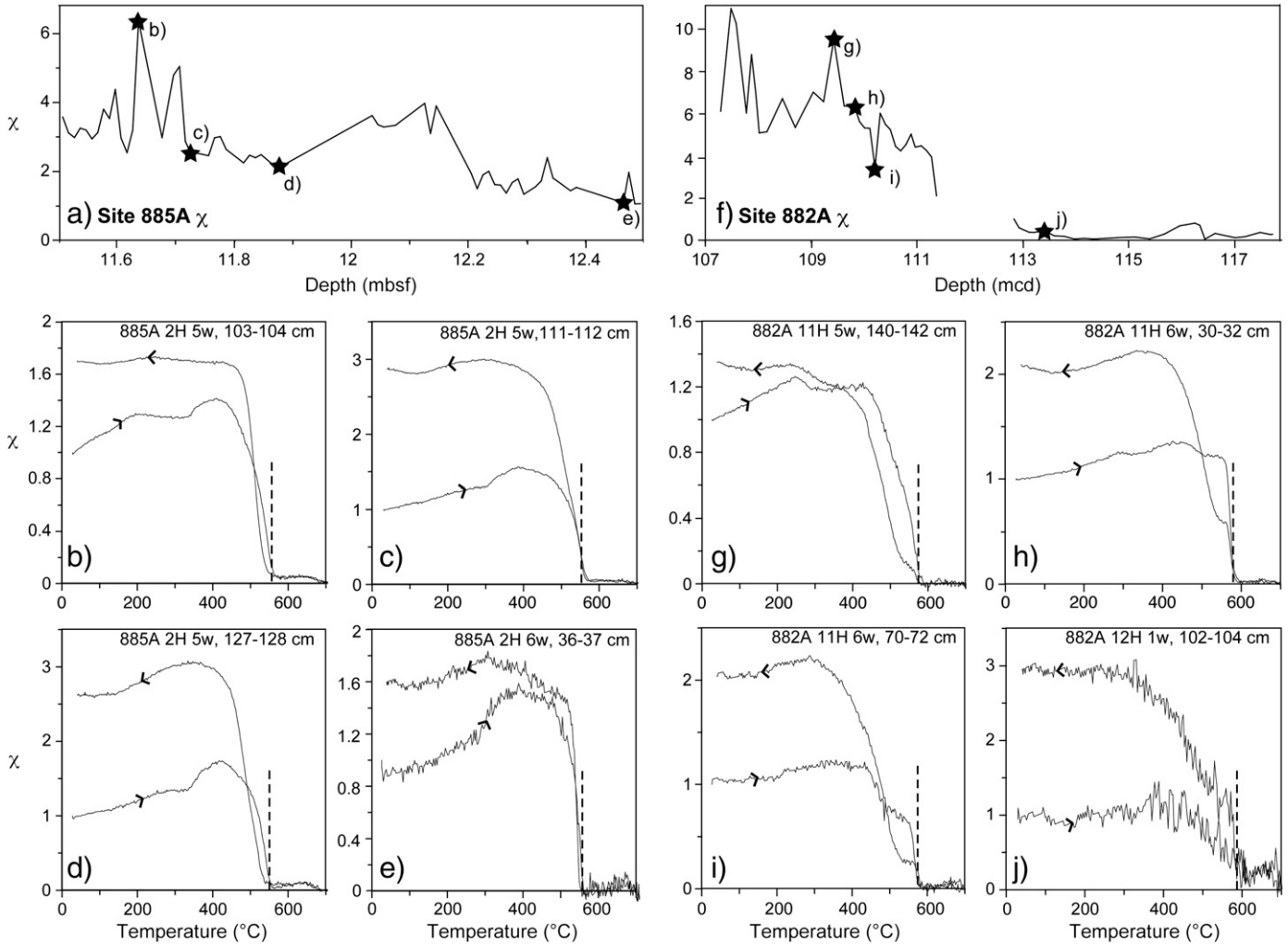

Fig. 3. Normalised χ–T curves for representative samples from ODP sites 885A (a–e) and 882A (f–j) (stars in (a) and (b) represent the positions of samples across the Plio-Pleistocene transition at ~2.75 Ma). Labels b–e and g–j indicate the positions of the samples. Dashed vertical lines (in b–e and g–j) mark the respective Curie temperatures, which indicate the dominance of magnetite and low-Ti titanomagnetite in each sample. The small high temperature component that decays at 680 °C indicates the presence of hematite. Arrows indicate warming and cooling cycles. The results indicate that the magnetic mineralogy does not change across ~2.75 Ma. The gradual increase of χ between room temperature and 200–300 °C is due to unblocking of fine-grained, including SP, particles. Above this temperature, the small change in slope is usually associated with transformation of maghemite into weakly magnetic hematite (Liu et al., 2005). Differences between the ratio of the final and initial χ reflect variable neoformation of magnetic minerals during heating and cooling, due to decomposition of silicate minerals (e.g., Liu et al., 2005).

concentration of magnetic particles rather than a change in magnetic mineral grain size. To first order, there is a positive correlation between χ, $IRM_{AF@100\ mT}$ and aeolian dust concentration (Fig. 2d). This strongly indicates that much of the low and high coercivity mineral content has an aeolian origin, with transportation from the Asian continental interior by prevailing westerlies (Rea et al., 1998). Nd and Sm analyses of Site 885 sediments indicate that terrigenous sediment deposited over the past 4 Ma is composed of a mixture of Asian dust and up to 35% volcanic ash (Pettke et al., 2000). Part of the late Pliocene χ increase at Site 885 is therefore likely also attributable to increased volcanic ash deposition.

Natural pedogenic hematite and goethite particles, which may be present in aeolian dust, often have Al substituted into the crystal lattice in place of Fe, which significantly influences both *HIRM* and the *S*-ratio (Liu et al., 2007). The *L*-ratio ($HIRM/IRM_{AF@100\ mT}$) was designed to identify coercivity variations that affect interpretations of standard parameters such as *HIRM* and the *S*-ratio (Liu et al., 2007). *HIRM* and the *S*-ratio can be interpreted conventionally only when the *L*-ratio is relatively stable. In contrast, if *HIRM* and the *L*-ratio are positively correlated, *HIRM* will not solely indicate changes in the absolute concentration of high coercivity minerals (Liu et al., 2007). At Site 885, the *L*-ratio remains stable at 13–12 mbsf (Fig. 2e), which indicates that the source of high coercivity minerals at ~2.75 Ma does not appear to change. In addition, the *S*-ratio (Fig. 2f) indicates that the relative contributions from low and high coercivity minerals remain almost constant during the χ increase at 2.75 Ma. The positive correlation between χ and χ_{fd} (Fig. 2a, b) across ash horizons (at ~5, 7.7, 9.2 and 9.6 mbsf) indicates that volcanic ash layers contain high concentrations of ultra-fine SP particles. The absence of correlation between χ and χ_{fd} across 12.6 mbsf therefore reflects that background inputs of aeolian magnetic particles are coarser-grained overall than the SP dominated magnetic particles found in near-pure ash horizons. Critically, whilst both the concentrations of aeolian dust and volcanic ash increased at Site 885 during iNHG, the χ increase appears to have involved simultaneous enrichment in the concentration of high and low coercivity magnetic minerals, with no change in the relative proportion of both types of mineral (sources) prior to the transition at 2.75 Ma.

Increased aeolian dust (Snoeckx et al., 1995; Sun et al., 2006) and volcanic ash (Prueher and Rea, 2001) inputs to the North Pacific Ocean in association with late Pliocene iNHG is well known. Our

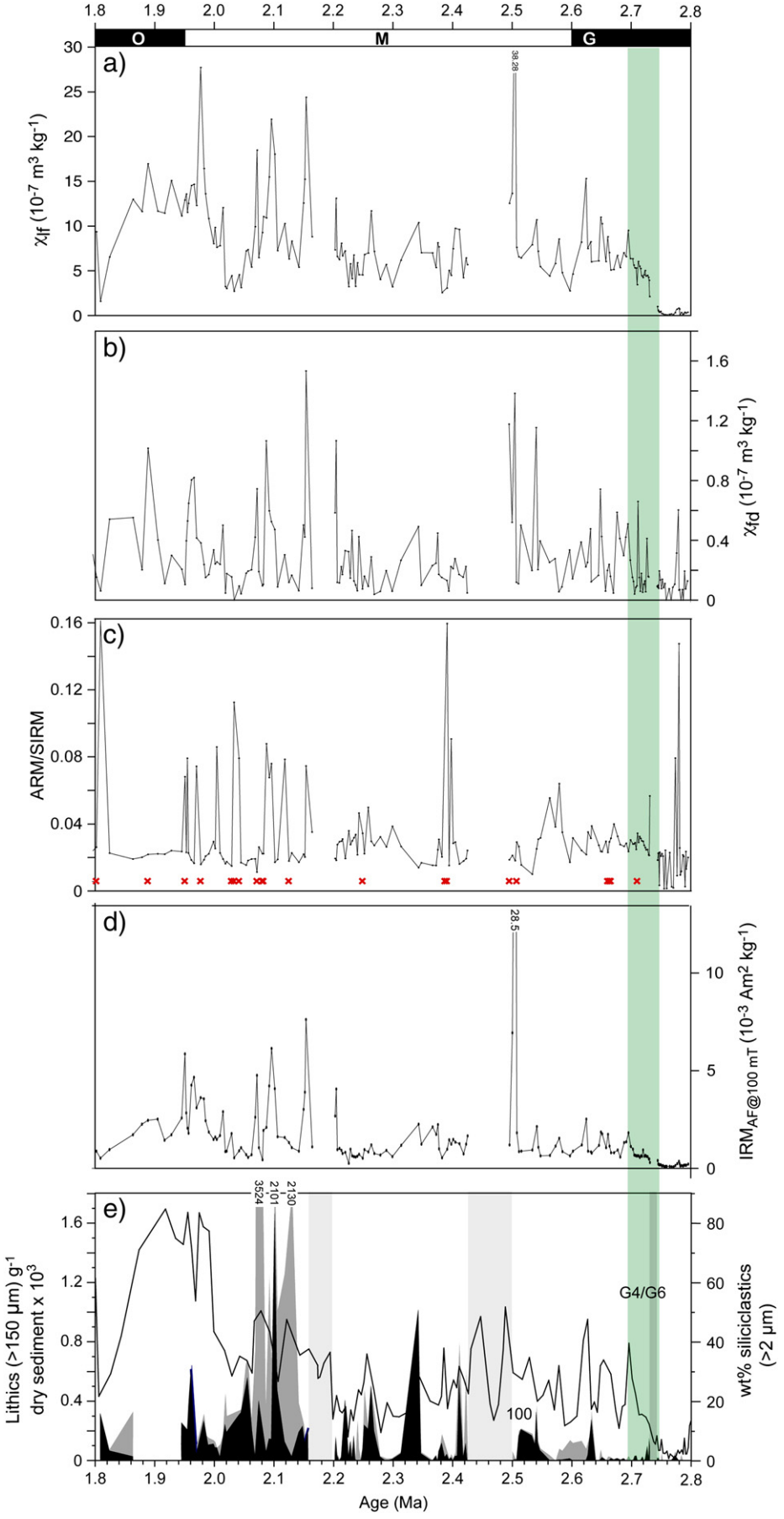
1.8 1.9 2.0 2.1 2.2 2.3 2.4 2.5 2.6 2.7 2.8
O
M
G
a)
38.29
χ_{lf} (10^{-7} m^3 kg^{-1})
b)
χ_{fd} (10^{-7} m^3 kg^{-1})
c)
ARM/SIRM
d)
28.5
$IRM_{AF@100\ mT}$ (10^{-3} Am^2 kg^{-1})
e)
3524
2101
2130
G4/G6
100
Lithics (>150 µm) g^{-1} dry sediment x 10^3
wt% siliciclastics (>2 µm)
Age (Ma)

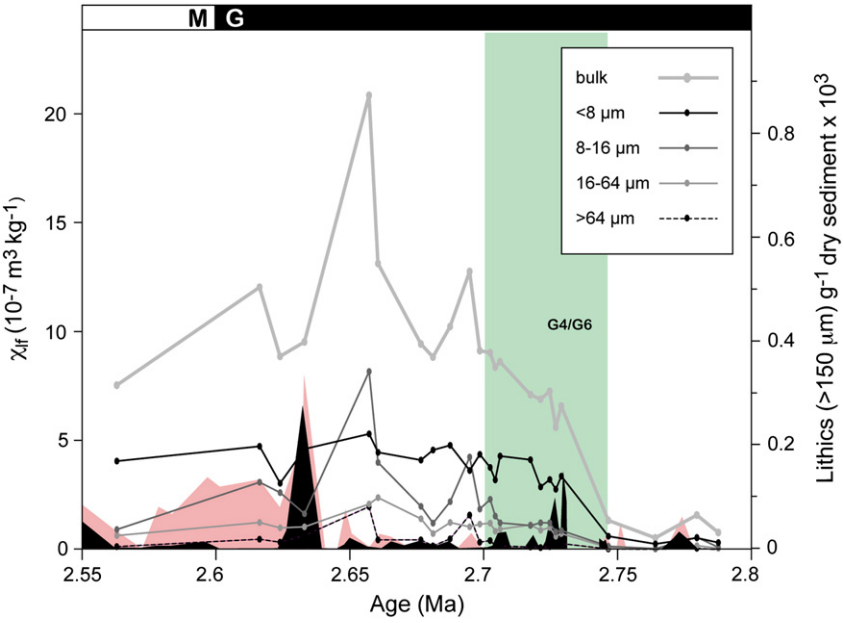

Fig. 5. Plots of low-field mass-specific magnetic susceptibility, χ_{lf}, for different grain size fractions across the interval of χ increase (~2.75 to 2.7 Ma). Also shown are counts of coarse (>150 μm) lithics per gramme of dry sediment. Black (red) filled peaks indicate lithic grains excluding (including) fresh volcanic glass. The vertical green bar indicates the Plio-Pleistocene palaeoclimatic transition across ~2.75 Ma. Variability in bulk χ is dominated by magnetic particles in the <8 μm, 8–16 μm and 16–64 μm grain-size fractions. Several short-term peaks are controlled by variability of magnetic properties of the 16–64 μm (at ~2.69, 2.66, and 2.6 Ma) and >64 μm (at ~2.69 and 2.66 Ma) fractions. However, most of the magnetic increase across ~110–113.5 mcd resides in the <8 μm fraction, with little or no increase in χ across this interval in the coarser grain-size fractions. The black/white bar at the top of the figure denotes the Gauss/Matuyama palaeomagnetic boundary (at 105.94 mcd) (Tiedemann and Haug, 1995; Weeks et al., 1995). Label G4/G6 = marine isotope stages.

environmental magnetic data from Site 885 demonstrate that these events, which were caused by increased aridity of the Asian continent (Janecek and Rea, 1983) and increased Kamchatka–Kurile and Aleutian Arc volcanism (Prueher and Rea, 2001) during iNHG, played an important role in enhancing χ of sediments from the central sub-Arctic North Pacific at ~2.75 Ma.

4.2. Coarse lithic counts and environmental magnetic records for ODP Site 882

The concentrations of coarse (>150 μm) lithics and χ are plotted for Site 882 from 2.8 to 1.8 Ma in Fig. 4. Although the structure of some glacial stages is obscure, coarse lithic abundance typically peaks every ~40 ka (Fig. 4e). Our χ record (Fig. 4a) reproduces the magnetic increase at ~113.5 m composite depth (mcd) (from ~2.75 Ma). Whilst χ, $IRM_{AF@100\ mT}$ and siliciclastic contents are consistently high since ~2.75 Ma (above ~113.5 mcd, Fig. 4a, d, e), peak coarse lithic concentration, which represents cold stages, nearly always returns to low baseline values before increasing again. This scenario is consistent with the episodic nature of ice rafting to other open ocean settings (e.g., the sub-polar North Atlantic Ocean; McManus et al. (1999)). Even if we consider that all fresh volcanic glasses were ice-rafted, coarse lithic concentration at Site 882 is still relatively low ($\ll$600 grains g^{-1}) throughout most of the studied stratigraphic interval.

If we take variability in coarse lithic flux (>150 μm, non fresh volcanic grains in cm^{-2} ka^{-1}) as an indicator of IRD deposition then our record suggests that although ice-rafting to Site 882 intensified at ~2.75 Ma, sustained coarse lithic fluxes, which are indicative of significant regional ice-sheet calving, are not a feature of glacials at Site 882 until ~2.55 Ma (since MIS 100) (Fig. 6c). For perspective, non Heinrich-event IRD flux rates of the >150 μm fraction for the Last Glacial northeast Atlantic Ocean were substantially larger, with typical values peaking at ~6 to 50×10^3 grains cm^{-2} ka^{-1} (Bond et al., 1992; Peck et al., 2007). Hence, whilst the first significant increase in coarse-grained IRD inputs occurred during MIS 100, the resultant lithic fluxes at Site 882 were low. These low fluxes are consistent with low-resolution records of coarse IRD mass accumulation rates (MARs) calculated previously for the late Pliocene at Site 882 (Prueher and Rea, 2001) and also at nearby Site 883 (Krissek, 1995; Prueher and Rea, 2001). These datasets confirm that during late Pliocene iNHG, IRD inputs north of the Pacific sub-Arctic front (i.e., at Site 881; Krissek 1995) were relatively low (McKelvey et al., 1995).

Environmental magnetic studies of Holocene Antarctic (Brachfeld and Banerjee, 2000), Last Glacial northeast Atlantic (Robinson et al., 1995) and Baffin Bay (Hall and King, 1989) sediments that contain abundant sand-sized IRD demonstrate that IRD strongly influences bulk sediment χ, so that coeval χ and IRD peaks are associated with a larger average magnetic particle size. In these areas, enhanced IRD inputs increase the concentration and relative proportion of lithogenic coarse-grained, multi-domain (MD) ferrimagnetic particles. Watkins et al. (2007) showed that the relationship between IRD and sediment magnetics is a function of source. Nevertheless, if increased

Fig. 4. Plots of late Pliocene magnetic and sedimentological properties of marine sediments from ODP Hole 882A on the time scale of Tiedemann and Haug (1995): (a) the low-field mass-specific magnetic susceptibility, χ_{lf}; (b) the frequency-dependent magnetic susceptibility, χ_{fd}; (c) *ARM/SIRM*; (d) $IRM_{AF@100\ mT}$; (e) counts of coarse (>150 μm) lithics per gramme of dry sediment. Black (grey) filled peaks indicate lithic grains excluding (including) fresh volcanic glass. The thin black line indicates the concentration (wt.%) of >2 μm siliciclastics (from Haug et al. (1995)). Typical coarse lithics encountered are dominated not only by quartz, feldspar and devitrified and fresh rhyolitic (but also minor basaltic) glass, but also variable numbers of volcanic and volcaniclastic, metamorphic, and siliciclastic rock fragments, hornblende and pyroxene. The grain types found are therefore consistent with those previously reported in Plio-Pleistocene sediments from this region (Conolly and Ewing, 1970; Kent et al., 1971; McKelvey et al., 1995). The vertical green bar indicates the Plio-Pleistocene palaeoclimatic transition across ~2.75 Ma. Vertical grey bars in (e) indicate sampling gaps in the composite stratigraphy. The black/white bar at the top of the figure denotes palaeomagnetic reversal boundaries (Tiedemann and Haug, 1995; Weeks et al., 1995): base of Olduvai Subchron = 84.42 mcd; Gauss/Matuyama boundary = 105.94 mcd. Red crosses in (c) denote data collected from ash layers. Note that coarse lithic count data in (e) excludes counts from sampled ash layers (n = 14). Labels 100 and G4/G6 = marine isotope stages.

IRD contributed significantly to bulk sediment χ during MIS G6 at Site 882, an unambiguous test of this relationship would be a strong correlation between χ, the concentration of sand-sized IRD and the grain-size of magnetic particles between ~2.75 and 2.7 Ma. However, our data suggest that such a relationship does not exist. The χ increase at ~2.75 Ma is broadly coincident with increased sand-sized IRD (Fig. 4e). However, the sharp reduction in IRD abundance (to <30 grains g^{-1}) soon after its initial increase (to ~150 grains g^{-1} at ~2.73 Ma), despite continued high values of χ (up to ~2.7 Ma), indicates that IRD is not mainly responsible for the χ elevation during MIS G6. Equally, *ARM/SIRM* (Fig. 4c), which should decrease when magnetic grain size increases, remains relatively unchanged, which indicates that χ at ~2.75 Ma does not mainly increase due to elevated deposition of coarse, MD ferrimagnetic grains.

Four further lines of evidence indicate that ice-rafting was not the dominant process contributing to χ at ~2.75 Ma. First, χ–T curves for representative samples from Site 882 (Fig. 3g–j) demonstrate that magnetite and low-Ti titanomagnetite dominates the χ signal. The consistency of the χ–T curves indicates that the magnetic minerals deposited did not significantly change across ~2.75 Ma at Site 882.

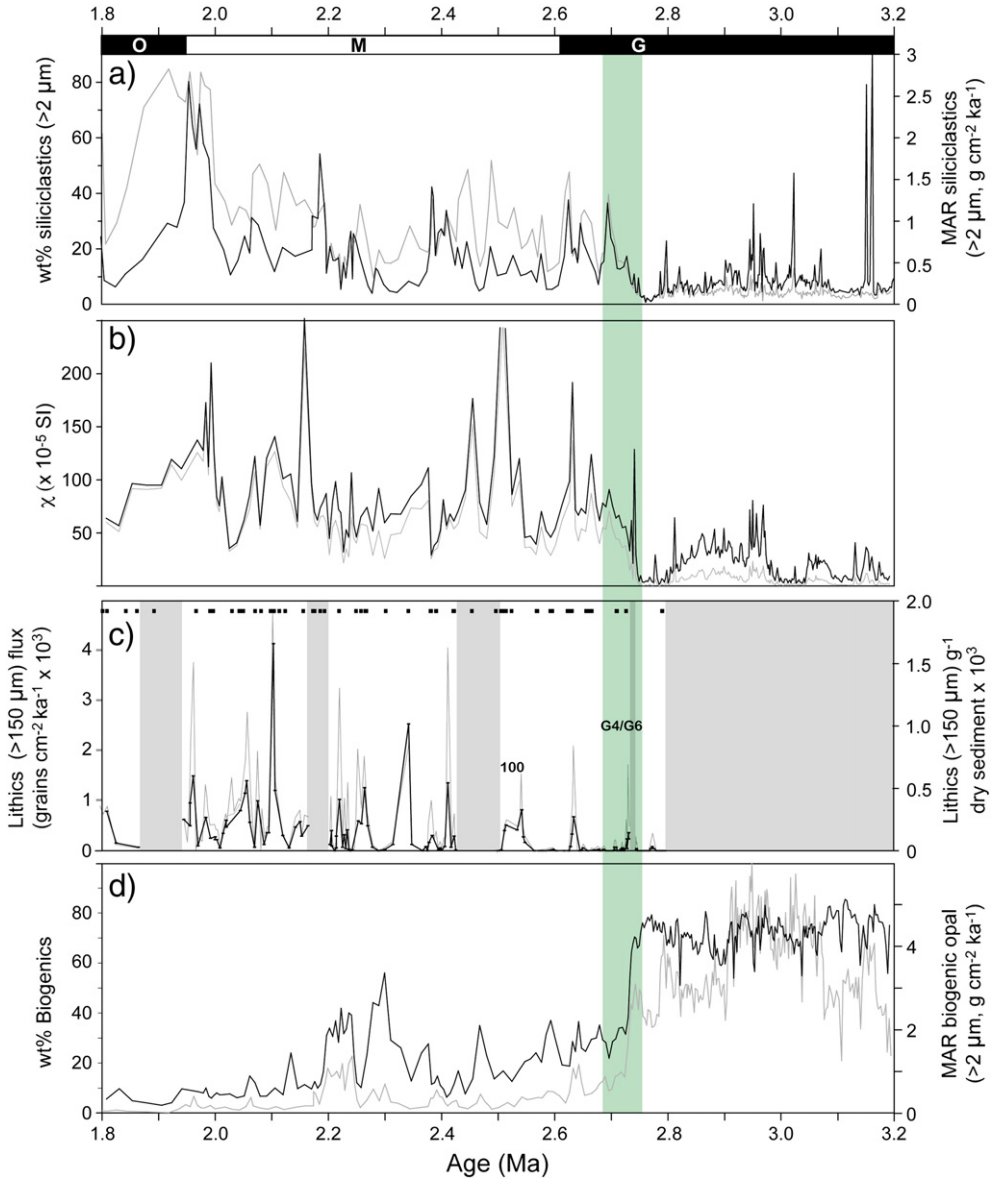

Fig. 6. Relationship between: (a) the mass accumulation (black line) and relative concentration of >2 µm siliciclastics (thin line) (Haug et al., 1995); (b) mass-specific magnetic susceptibility, χ (thin line), and biogenic-free χ (black line) (Shipboard Scientific Party, 1993); (c) ice-rafted debris, IRD, (>150 µm) per gramme of dry bulk sediment (black line) and IRD deposition rates (in grains cm^{-2} ka^{-1}, grey line), and (d) biogenic (wt.% carbonate and opal) concentration (black line) and mass accumulation (thin line) of biogenic opal (Haug et al., 1995) for Site 882 between 3.2 and 1.8 Ma (~178 and 82 mcd (Tiedemann and Haug, 1995)). The vertical green bar indicates the Plio-Pleistocene palaeoclimatic transition across ~2.75 Ma. Vertical grey bars in (c) indicate sampling gaps in the composite stratigraphy. Datasets shown in (b) and biogenic concentration data in (d) have been re-sampled at common 10 ka intervals. The effects of biogenic dilution on bulk sediment χ are normalised by expressing χ on a biogenic-free basis ({χ/[100% − biogenic wt.%] × 100} (Robinson et al., 1995)). χ in (b) and coarse lithic count data (n = 14) in (c) excludes data from ash layers. Coarse lithic fluxes were calculated following Peck et al. (2007). Sedimentation rates were estimated from the Site 882 astronomical age model (Tiedemann and Haug, 1995) and dry-bulk densities from shipboard determined GRAPE wet-bulk density data following Maslin et al. (1995). Black squares in (c) represent the midpoint depth of discrete tephra identified in this study from intervals of shipboard core images that correspond to the Site 882 splice (Tiedemann and Haug, 1995). Labels 100 and G4/G6 = marine isotope stages.

Second, the χ increase between ~2.75 and 2.7 Ma is mainly controlled by magnetic minerals in the fine (<8 μm) fraction rather than the coarse (>64 μm) sediment fraction (Fig. 5). Third, a plot of biogenic-free bulk χ (Fig. 6b) indicates significant χ increases prior to the onset of region-wide IRD deposition at ~2.75 Ma (Krissek, 1995). Fourth, published >2 μm siliciclastic MARs for Site 882 (Fig. 6a) (Haug et al., 1995) indicate that whilst terrigenous inputs increase at ~2.75 Ma, the pre-MIS G6 χ peaks are coincident with siliciclastic inputs that are also comparable in magnitude to those between ~2.75 and 2.55 Ma.

The magnitude of the Site 882 χ increase is comparable to the χ increase at Site 885, which we attribute to a terrigenous enrichment of Site 885 sediments by a mixture of aeolian dust and volcanic ash. Low-resolution records of volcanic ash deposition at Site 882 (Prueher and Rea, 2001) and other sedimentological analyses (Krissek, 1995) indicate that disseminated silt-sized volcanic ash makes a sizable contribution (~100–300 mg cm^{-2} ka^{-1}) to >2 μm siliciclastic inputs and χ from ~2.75 Ma. Several χ peaks for the 8–64 μm bulk sediment fraction (Fig. 5) likely reflect the presence of magnetite associated with disseminated fresh volcanic glass (which is not evident in our coarse lithic counts). Generally, the samples can be divided into two groups based on *ARM*/χ (Fig. S1a) and *ARM*/*SIRM* ratios (Fig. S1b). The *ARM*/*SIRM* record indicates that the relatively finer grained magnetic particles in group 1 (peaks >0.07) dominate episodically the mineral magnetic properties (Fig. S1c). Three of the *ARM*/*SIRM* peaks correspond to distinct ash horizons. The remaining peaks likely correspond to high disseminated volcanic glass concentrations (Prueher and Rea, 2001). Not all ash layers visible in core photographs correspond to *ARM*/*SIRM* anomalies. This probably indicates variable magnetic mineralogy in the ash layers.

As for Site 885, we propose that a large portion of magnetic particles in group 2 samples that are responsible for the χ increase at Site 882 reside in a previously overlooked mixture of aeolian dust and disseminated volcanic ash. Whilst IRD abundance intensified from ~2.75 Ma, increased relative contributions from volcanism and dust deposition to the increase in clay through sand-sized terrigenous sediment fraction at ~2.75 Ma indicates that χ cannot be used as a simple IRD proxy at Site 882. Given the fine-grained nature of Site 882 siliciclastics and the strong correlation between MARs on the Chinese Loess Plateau and Site 882 terrigenous inputs (Fig. 7) it is also reasonable to hypothesise that Site 882 terrigenous inputs reflect relative changes in aeolian dust inputs at Site 882 (see also Supplementary discussion).

4.3. Late Pliocene dust deposition and nutrient use at site 882

Aeolian dust and volcanic ash supply to the oceans is important for biogeochemical cycles because these materials represent a sizable source of soluble Fe to the euphotic zone (Duggen et al., 2010; Fung et al., 2000). Fe can be an important limiting factor for phytoplankton growth and for macro-nutrient consumption (e.g., nitrate and phosphate) (Harrison et al., 1999; Martin et al., 1990; Moore et al., 2009).

That opal burial decreased at Site 882, with a synchronous increase in $\delta^{15}N_{bulk}$ (Sigman et al., 1999) and a decrease in $\delta^{30}Si_{diatom}$ (Reynolds et al., 2008) during a time of increased aeolian dust and volcanic ash inputs is important for understanding the mechanisms responsible for this chain of events (Fig. 8). Variations in $\delta^{30}Si_{diatom}$ and $\delta^{15}N_{bulk}$ should co-vary, even though $\delta^{15}N$ measurements are from bulk sediment which are more susceptible to water column and post-depositional alteration than diatom $\delta^{15}N$ (De La Rocha, 2006). However, changes in $\delta^{30}Si_{diatom}$ $\delta^{15}N_{bulk}$ at 2.73 Ma are anti-correlated (Fig. 8). This anti-correlation has been attributed to increased Si:N of bioavailable nutrients supplied to the photic zone and/or to a change in silicic acid $\delta^{30}Si$ (Reynolds et al., 2008). Whilst these explanations can account for changes in $\delta^{30}Si_{diatom}$ and $\delta^{15}N_{bulk}$ at 2.73 Ma, the extent to which a nutrient may act as the limiting factor for diatom growth in the stratified water column provides a simpler explanation.

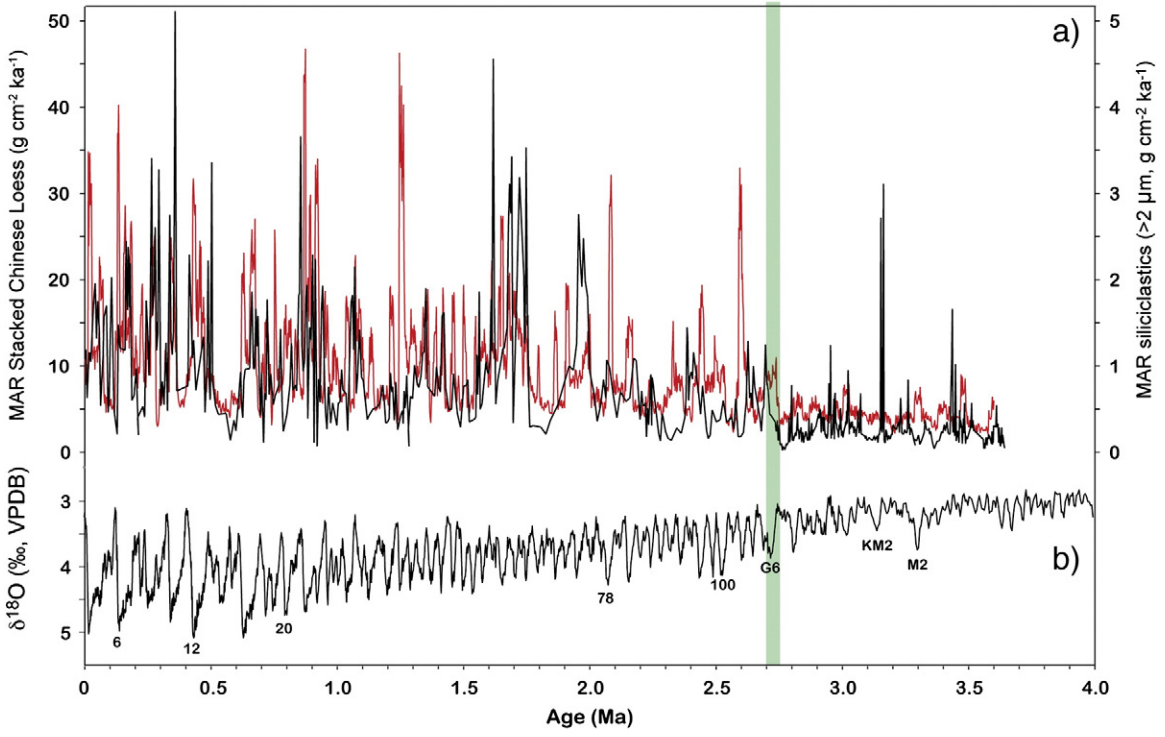

Fig. 7. Relationship between mass accumulation rates (MARs) of: (a) Chinese Loess Plateau dust stack (red line; Sun and An, 2005) and Site 882 >2 μm siliciclastics (black line; Haug et al., 1995), and (b) the global benthic oxygen isotope stack (LR04; Lisiecki and Raymo, 2005) for the past 3.5 Ma. Data are plotted on the respective published age models. Labels in (b) = marine isotope stages.

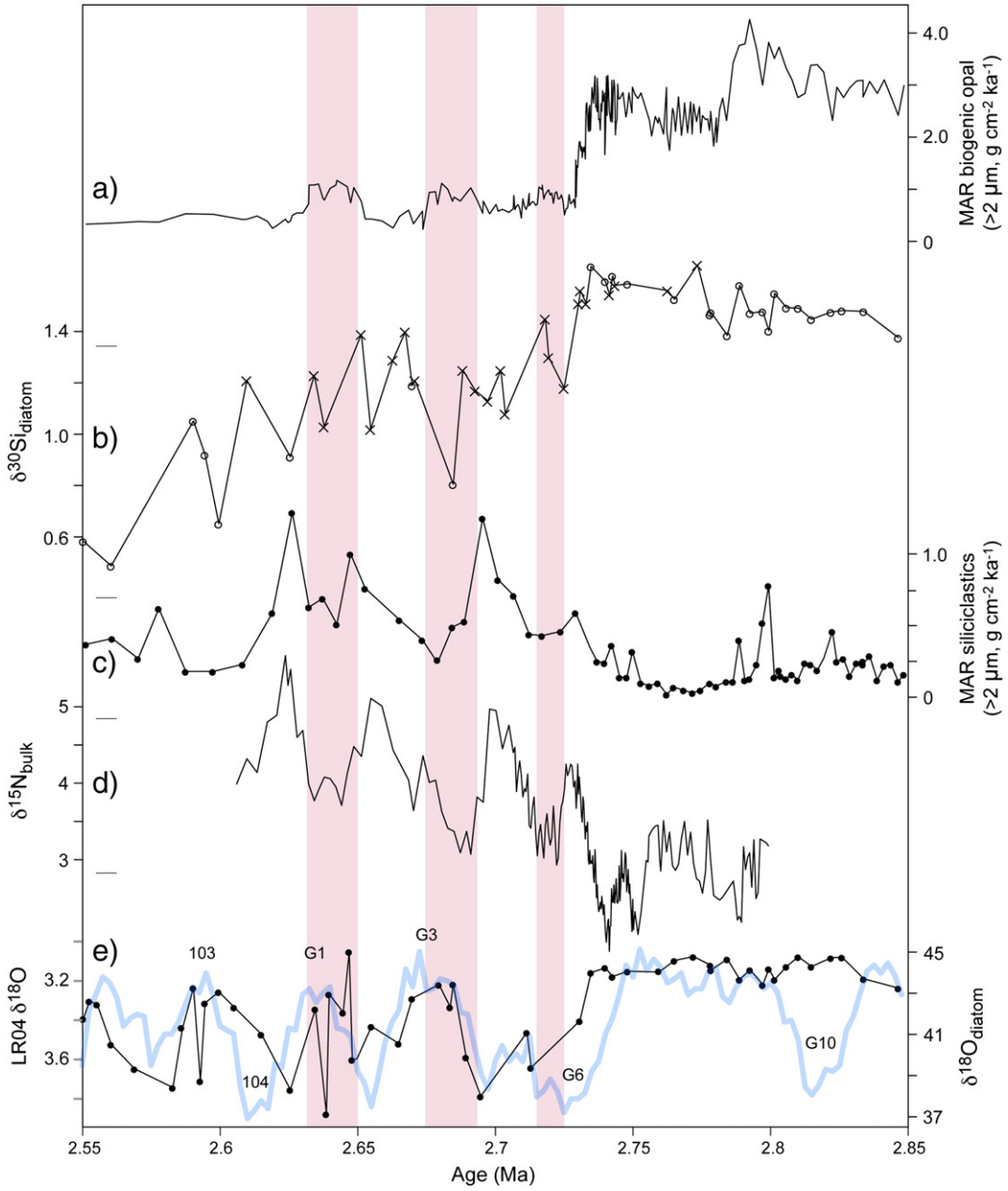

Fig. 8. Relationship between: (a) mass accumulation of opal (Haug et al., 1999; Sigman et al., 2004), (b) $\delta^{30}Si_{diatom}$ data generated in this study (open circles) and from Reynolds et al. (2008) (crosses), (c) the mass accumulation of >2 μm siliciclastics (Haug et al., 1995), (d) $\delta^{15}N_{bulk}$ (Sigman et al., 2004) and (e) $\delta^{18}O_{diatom}$ (Swann, 2010; Swann et al., 2006) and LR04 global benthic $\delta^{18}O$ foraminiferal stack (transparent blue line) (Lisiecki and Raymo, 2005) during the onset of major northern hemisphere glaciation (labels = MIS). The age models used are from the respective studies. Following Reynolds et al. (2008), the age of LR04 has been adjusted by + 10 ka to position the Matuyama/Gauss boundary at 2.61 Ma on the orbital time scale (Deino et al., 2006). The vertical pink bars highlight minima in $\delta^{15}N_{bulk}$ discussed in Section 4.3.

High/low levels of $\delta^{30}Si_{diatom}/\delta^{15}N_{bulk}$ prior to 2.73 Ma suggest that silicic acid use was considerably more complete than nitrate use during periods of unimpeded deep-water upwelling. The switch to a stratified system after this interval would have created a finite supply of photic zone nutrients capable of supporting a limited diatom population before one or more nutrients became limiting and inhibited further productivity. For example, at present, ignoring issues of light, the availability of silica, nitrate, phosphorous and iron are estimated to limit diatom growth for 11%, 50%, 1%, 39% of the world's ocean, respectively (Moore et al., 2002). In this case, the increase in $\delta^{15}N_{bulk}$ after 2.73 Ma suggests that nitrate may have become the limiting nutrient for diatom growth. This could have occurred by decreasing nitrate flux to surface waters relative to silicic acid, in agreement with Reynolds et al. (2008), with the increased amplitude of $\delta^{15}N_{bulk}$ and $\delta^{30}Si_{diatom}$ variations after MIS G6 reflecting a change in the Si:N ratio of nutrients supplied to the photic zone over orbital timescales. With no evidence for a breakdown in halocline stratification following MIS G6 (Swann, 2010), this could have occurred through orbital changes in nutrient composition and strength of deep-water circulation (Reynolds et al., 2008). Reynolds et al. (2008) did not consider the possibility of an Fe-induced change in Si:N export ratio at Site 882, stating that any increased Fe availability should raise rather than lower opal productivity at 2.73 Ma. However, they did not consider that a drop in photic zone nitrate and silicic acid supply following stratification would significantly lower productivity

regardless of changes in Fe input. Unlike the Southern Ocean, the sub-Arctic Pacific obtains most of its Fe from atmospheric aerosol deposition (Martin and Gordon, 1988; Somes et al., 2010). We therefore instead propose that halocline development led to the drop in opal MAR whilst the concordant increase in Fe deposition raised biological demand for nitrate relative to silicic acid (Hutchins and Bruland, 1998; Takeda, 1998). It is difficult to know whether most of the biovailable Fe delivered to Site 882 was sourced from aeolian dust or volcanic ash. Regardless, combined with reduced nutrient availability, we propose that increased Fe would have caused near complete nitrate consumption (high $\delta^{15}N_{bulk}$) and driven the system to nitrate limitation, causing silicic acid to be under-used (indicated by low $\delta^{30}Si_{diatom}$).

The long-term increase in $\delta^{15}N_{bulk}$ and decrease in $\delta^{30}Si_{diatom}$ from 2.73 to 2.55 Ma further indicates that nitrate limitation increased with time, resulting in greater under use of silicic acid. This chain of events can explain the observed anti-phase changes in $\delta^{15}N_{bulk}$ and $\delta^{30}Si_{diatom}$ without invoking changes in composition or relative concentration of deep-water nutrients delivered to the photic zone, although such changes could still have occurred. Our explanation supports the idea that Fe inputs to the North Pacific over the last 800 ka could have driven the biological system to limitation by a nutrient other than Fe (Kienast et al., 2004) and suggests that Fe limitation in the modern ocean (Tsuda et al., 2003) is not always typical of past conditions. Although the resolution of siliciclastic MAR data is not high, the strong positive relationship between $\delta^{15}N_{bulk}$ and late Pliocene >2 μm siliciclastic MARs ($R^2 = +0.72$, $n = 46$, $p < 0.01\%$) supports a close link between Fe inputs and nitrate use especially from ~2.73 Ma (Fig. 8). Short-term variations in $\delta^{15}N_{bulk}$ and $\delta^{30}Si_{diatom}$ after 2.73 Ma may therefore reflect changes in Fe supply and biological demand for nitrate and silicic acid. The absence of a clear relationship between siliciclastic and opal MARs, $\delta^{15}N_{bulk}$ and $\delta^{30}Si_{diatom}$ prior to MIS G6 when terrigenous inputs were non-zero, suggests that Fe addition was insufficient to noticeably alter the demand for nitrate and silicic acid when nutrient-rich deep-waters were vigorously upwelled.

Of note in the post-2.73 Ma record are three intervals of low $\delta^{15}N_{bulk}$ (Fig. 8, pink bars). Each coincides with reduced siliciclastic (Fe) input and a small increase in opal MAR. For the first interval, the resolution of the $\delta^{18}O_{diatom}$ record of Swann (2010) is insufficient to make comparisons. For the second and third intervals, however, increased opal MAR and minima in $\delta^{15}N_{bulk}$ coincide with higher $\delta^{18}O_{diatom}$ values, and are linked to reduced freshwater input during interglacials when the water column came close to overturning the stratification (Swann, 2010). Weakening of stratification during these periods may have increased upward diffusion of deep-water nutrients, leading to the observed increase in opal MAR. We suggest that the opal increase was retarded by reduced aeolian Fe input, leading to Fe rather than nitrate limitation of surface waters. This process can explain observed trends in the Site 882 isotope data by reducing relative rates of nitrate use (lower $\delta^{15}N_{bulk}$), but maintaining similarly low silicic acid use as was the case in the nitrate-limited water column from 2.73 Ma.

5. Conclusions

We present new high-resolution lithic grain counts and environmental magnetic data from ODP Sites 882 and 885, which record Plio-Pleistocene ice-rafting to the sub-Arctic Pacific Ocean and the widely observed χ increase in sub-Arctic Pacific sediment at ~2.75 Ma, respectively. Although sand-sized IRD concentration increases during cold stages from ~2.75 Ma, its abundance is relatively low until 2.55 Ma. At Site 882, neither IRD abundance nor magnetic particle grain size increase in accordance with χ across MIS G6, which suggests that ice-rafting was not mainly responsible for the χ elevation at ~2.75 Ma. Instead, we propose that the observed χ elevation of sub-Arctic northwest Pacific sediments is mainly due to increased deposition of fine-grained ferrimagnetic particles in dust and volcanic ash during the late Pliocene iNHG. This conclusion is supported by our magnetic study of Site 885 sediments, which lies downwind of Site 882.

Our findings reveal a close link between Fe inputs and surface water nutrient use at Site 882, following development of the North Pacific halocline. We propose that following stratification at 2.73 Ma, substantially lower macronutrient concentrations reduced opal productivity, but elevated aeolian (and potentially volcanic) Fe inputs increased biological demand for NO_3^- relative to $Si(OH)_4$. This resulted in near-complete NO_3^- consumption and drove the system to nitrate limitation. This caused the pool of $Si(OH)_4$ to be under-used. Our explanation is supported by published $\delta^{15}N$ and $\delta^{30}Si$ records and by our silicon isotope data. Our findings also suggest that Fe limitation in the modern ocean is not always typical of past conditions.

Supplementary materials related to this article can be found online at doi:10.1016/j.epsl.2011.05.029.

Acknowledgements

This research used samples provided by the ODP, which was sponsored by the US National Science Foundation and participating countries under management of the Joint Oceanographic Institutions, Inc. We thank P.D. deMenocal for editorial handling and we also thank P. Rumford at the Gulf Coast Core Repository for sediment sampling, E.J. Rohling for comments on an earlier version of the manuscript and two anonymous reviewers whose comments improved the paper. QL acknowledges support from Marie Curie Fellowship (IIF) proposal 7555, additional support from NSFC (41025013 and 40821091) and the '100 Talent Program' of the Chinese Academy of Science. GEAS was funded by NERC post-doctoral fellowship NE/F012969/1.

References

Arnold, E., Leinen, M., King, J.W., 1995. Paleoenvironmental variation based on the mineralogy and rock-magnetic properties of sediment from Sites 885 and 886. Proc. ODP, Sci. Res. 145, 231–245.

Bailey, I., Bolton, C.T., DeConto, R.M., Pollard, D., Schiebel, R., Wilson, P.A., 2010. A low threshold for North Atlantic ice rafting from "low-slung slippery" late Pliocene ice sheets. Paleoceanography 25 (PA1212). doi:10.1029/2009PA001736.

Bigg, G.R., Clark, C.D., Hughes, A.L.C., 2008. Last glacial ice sheet on the Pacific Russian coast and catastrophic change arising from coupled ice-volcanic interaction. Earth Planet. Sci. Lett. 265, 559–570.

Bloemendal, J., deMenocal, P., 1989. Evidence for a change in the periodicity of tropical climate cycles at 2.4 Myr from whole-core magnetic susceptibility measurements. Nature 342, 897–900.

Bond, G.C., Heinrich, H., Broecker, W., Labeyrie, L., McManus, J., Andrew, J., Huon, S., Jantschik, R., Clasen, S., Simet, C., Tedesco, K., Klas, M., Bonani, G., Ivy, S., 1992. Evidence for massive discharges of icebergs into the North Atlantic ocean during the last glacial period. Nature 360, 245–249.

Brachfeld, S.A., Banerjee, S.K., 2000. Rock-magnetic carriers of century-scale susceptibility cycles in glacial-marine sediments from the Palmer Deep, Antarctic Peninsula. Earth Planet. Sci. Lett. 176, 443–455.

Brzezinski, M.A., Pride, C.J., Franck, V.M., Sigman, D.M., Sarmiento, J.L., Matsumoto, K., Gruber, N., Rau, G.H., Coale, K.H., 2002. A switch from $Si(OH)_4$ to NO_3 depletion in the glacial Southern Ocean. Geophys. Res. Lett. 29, 1564. doi:10.1029/2001GL014349.

Clemens, S.C., Prell, W.L., 1991. One million year record of summer monsoon winds and continental aridity from the Owen Ridge (site 722), Northwest Arabian Sea. Proc. ODP, Sci. Res. 117, 365–388.

Conolly, J.R., Ewing, M., 1970. Ice-rafted detritus in Northwest Pacific deep-sea sediments. In: Hays, J.D. (Ed.), Geological Investigations of the North Pacific: Geol. Soc. Am. Mem., 126, pp. 219–231.

Crosta, X., Shemesh, A., 2002. Reconciling down-core anticorrelation of diatom carbon and nitrogen isotopic ratios from the Southern Ocean. Paleoceanography 17, 1010. doi:10.1029/2000PA000565.

De La Rocha, C.L., Brzezinski, M.A., DeNiro, M.J., Shemesh, A., 1998. Silicon-isotope composition of diatoms as an indicator of past oceanic change. Nature 395, 680–683.

De La Rocha, C.L., 2006. Opal-based isotopic proxies of paleoenvironmental conditions. Global Biogeochem. Cycles 20 (GB4S09). doi:10.1029/2005GB002664.

Deino, A.L., Kingston, J.D., Glen, J.M., Edgar, R.K., Hill, A., 2006. Precessional forcing of lacustrine sedimentation in the late Cenozoic Chemeron Basin, Central Kenya Rift, and calibration of the Gauss/Matuyama boundary. Earth Planet. Sci. Lett. 247, 41–60.

deMenocal, P., Bloemendal, J., King, J.W., 1991. A rock-magnetic record of monsoonal dust deposition at 2.4 Ma. Proc. ODP, Sci. Res. 117, 389–407.

Dickens, G.R., Snoeckx, H., Arnold, E., Morley, J.J., Owen, R.M., Rea, D.K., Ingram, L., 1995. Composite depth scale and stratigraphy for Sites 885/886. Proc. ODP, Sci. Res. 145, 205–217.
Doh, S.J., King, J.W., Leinen, M., 1988. A rock-magnetic study of giant piston Core LL44-GPC3 from the central North Pacific and its paleoceanographic implications. Paleoceanography 3, 89–111.
Duce, R.A., et al., 1991. The atmospheric input of trace species to the world ocean. Global Biogeochem. Cycles 5, 193–259.
Duggen, et al., 2010. The role of airborne volcanic ash for the surface ocean biogeochemical iron-cycle: a review. Biogeosciences 7, 827–844.
Evans, M.E., Heller, F., 2003. Environmental Magnetism: Principles and Applications of Enviromagnetics. Academic Press. 299 pp.
Frank, M., Gersonde, R., Rugers van der Loeff, M., Bohrmann, G., Nürnberg, C.C., Kubik, P.W., Suter, M., Mangini, A., 2000. Similar glacial and interglacial export bioproductivity in the Atlantic sector of the Southern Ocean: multiproxy evidence and implications for glacial atmospheric CO_2. Paleoceanography 15, 642–658.
Fung, I.Y., Meyn, S.K., Tegen, I., Doney, S.C., John, J.G., Bishop, J.K.B., 2000. Iron supply and demand in the upper ocean. Global Biogeochem. Cycles 14, 281–295.
Grousset, F.E., Labeyrie, L., Sink, J.A., Cremer, M., Bond, G., Duprat, E., Cortijo, E., Huon, S., 1993. Patterns of ice-rafted detritus in the glacial north Atlantic (40–55°N). Paleoceanography 8, 175–192.
Hall, F.R., King, J.W., 1989. Rock-magnetic stratigraphy of Site 645 (Baffin Bay) from ODP Leg 105. In: Srivastava, S.P., Arthur, M., Clement, B.M. (Eds.), Proc. ODP, Sci. Res., 105, pp. 843–859.
Hamme, R.C., et al., 2010. Volcanic ash fuels anomalous plankton bloom in subarctic northeast Pacific. Geophys. Res. Lett. 37, L19604. doi:10.1029/2010GL044629.
Harrison, P.J., Boyd, P.W., Varela, D.E., Takeda, S., Shiomoto, A., Odate, T., 1999. Comparison of factors controlling phytoplankton productivity in the NE and NW subarctic Pacific gyres. Progr. Oceanogr. 43, 205–234.
Haug, G.H., Maslin, M.A., Sarnthein, M., Stax, R., Tiedemann, R., 1995. Evolution of Northwest Pacific sedimentation patterns since 6 Ma (Site 882). In: Rea, D.K., Basov, I.A., Scholl, D.W., Allan, J.F. (Eds.), Proc. ODP, Sci. Res., 145, pp. 293–314.
Haug, G.H., Sigman, D.M., Tiedemann, R.T., Pedersen, F., Sarnthein, M., 1999. Onset of permanent stratification in the subarctic Pacific Ocean. Nature 401, 779–782.
Haug, G.H., Ganopolski, A., Sigman, D.M., Rosell-Mele, A., Swann, G.E.A., Tiedemann, R., Jaccard, S.L., Bollmann, J., Maslin, M.A., Leng, M.J., Eglinton, G., 2005. North Pacific seasonality and the glaciation of North America 2.7 million years ago. Nature 433, 821–825.
Hemming, S.R., 2004. Heinrich events: massive late Pleistocene detritus layers of the North Atlantic and their global climate imprint. Rev. Geophys. 42 (RG1005). doi:10.1029/2003RG000128.
Hoffmann, L.J., Peeken, I., Lochte, K., 2007. Effects of iron on the elemental stoichiometry during EIFEX and in the diatoms *Fragilariopsis kerguelensis* and *Chaetoceros dichaeta*. Biogeosciences 4, 569–579.
Hutchins, D., Bruland, K.W., 1998. Iron-limited growth and Si:N uptake ratios in a coastal upwelling regime. Nature 393, 561–564.
Iwamoto, Y., Yumimoto, K., Toratani, M., Tsuda, A., Miura, K., Uno, I., Uematsu, M., 2011. Biogeochemical implications of increased mineral particle concentrations in surface waters of the northwestern North Pacific during an Asian dust event. Geophys. Res. Lett. 38, L01604. doi:10.1029/2010GL045906.
Janecek, T.R., Rea, D.K., 1983. Eolian deposition in the northeast Pacific Ocean: Cenozoic history of atmospheric circulation. Geol. Soc. Am. Bull. 94, 730–738.
Kent, D.V., Opdyke, N.D., Ewing, M., 1971. Climate change in the North Pacific using ice-rafted detritus as a climatic indicator. Geol. Soc. Am. Bull. 82, 2741–2754.
Kienast, S.S., Hendy, I.L., Crusius, J., Pedersen, T.F., Calvert, S.E., 2004. Export production in the Subarctic North Pacific over the last 800 kyr: no evidence for iron fertilisation. J. Oceanogr. 60, 189–203.
King, J.W., Channell, J.E.T., 1991. Sedimentary magnetism, environmental magnetism, and magnetostratigraphy. Rev. Geophys., Suppl., US National Report to IUGG, pp. 358–370.
Kleiven, H.F., Jansen, E., Fronval, T., Smith, T.M., 2002. Intensification of Northern Hemisphere glaciations in the circum Atlantic region (3.5–2.4 Ma) — ice-rafted detritus evidence. Palaeogeogr. Palaeoclimatol. Palaeoecol. 184, 213–223.
Krissek, L.A., 1995. Late Cenozoic ice-rafting records from Leg 145 sites in the North Pacific: late Miocene onset, late Pliocene intensification, and Pliocene–Pleistocene events. In: Rea, D.K., Basov, I.A., Scholl, D.W., Allan, J.F. (Eds.), Proc. ODP, Sci. Res., 145, pp. 179–194.
Larrasoaña, J.C., Roberts, A.P., Rohling, E.J., 2008. Magnetic susceptibility of eastern Mediterranean marine sediments as a proxy for Saharan dust supply? Mar. Geol. 254, 224–229.
Larrasoaña, J.C., Roberts, A.P., Rohling, E.J., Winklhofer, M., Wehausen, R., 2003. Three million years of monsoon variability over the northern Sahara. Clim. Dyn. 21, 689–698.
Lawrence, K.T., Herbert, T.D., Brown, C.M., Raymo, M.E., Haywood, A.M., 2009. High-amplitude variations in North Atlantic sea surface temperature during the early Pliocene warm period. Paleoceanography 24 (PA2218). doi:10.1029/2008PA001669.
Leng, M.J., Sloane, H.J., 2008. Combined oxygen and silicon isotope analysis of biogenic silica. J. Quat. Sci. 23, 313–319.
Lisiecki, L.E., Raymo, M.E., 2005. A Pliocene Pleistocene stack of 57 globally distributed benthic delta-18O records. Paleoceanography 20, L23605. doi:10.1029/2005PA001164.
Liu, Q., Deng, C.L., Yu, Y.J., Torrent, J., Jackson, M.J., Banerjee, S.K., Zhu, R., 2005. Temperature dependence of magnetic susceptibility in an argon environment: implications for pedogenesis of Chinese loess/palaeosols. Geophys. J. Int. 161, 102–112.
Liu, Q., Roberts, A.P., Torrent, J., Horng, C.-S., Larrasoaña, J.C., 2007. What do the HIRM and S-ratio really measure in environmental magnetism? Geochem. Geophys. Geosyst. 8, Q09011. doi:10.1029/2007GC001717.
Maher, B.A., Thompson, R., 1999. Quaternary Climates, Environments and Magnetism. Cambridge University Press. 390 pp.
Martin, J.H., Gordon, R.M., 1988. Northeast Pacific iron distributions in relation to phytoplankton productivity. Deep Sea Res. 35, 177–196.
Martin, J.H., Fitzwater, S.E., Gordon, R.M., 1990. Iron deficiency limits growth in Antarctic waters. Global Biogeochem. Cycles 4, 5–12.
Maslin, M.A., Haug, G.H., Sarnthein, M., Tiedemann, R., Erlenkeuser, H., Stax, R., 1995. Northwest Pacific Site 882: the initiation of Northern Hemisphere glaciation. In: Rea, D.K., Basov, I.A., Scholl, D.W., Allan, J.F. (Eds.), Proc. ODP, Sci. Res., 145, pp. 315–329.
Maslin, M.A., Li, X.S., Loutre, M.-F., Berger, A., 1998. The contribution of orbital forcing to the progressive intensification of Northern Hemisphere glaciation. Quat. Sci. Rev. 17, 411–426.
Matsumoto, K., Sarmiento, J.L., 2008. A corollary to the silicic acid leakage hypothesis. Paleoceanography 23 (PA2203). doi:10.1029/2007PA001515.
Matsumoto, K., Sarmiento, J.L., Brzezinski, M.A., 2002. Silicic acid leakage from the Southern Ocean: a possible explanation for glacial atmospheric pCO_2. Global Biogeochem. Cycles 16, 1031. doi:10.1029/2001GB001442.
McKelvey, B.C., Chen, W., Arculus, R.J., 1995. Provenance of Pliocene–Pleistocene ice-rafted debris, Leg 145, Northern Pacific Ocean. In: Rea, D.K., Basov, I.A., Scholl, D.W., Allan, J.F. (Eds.), Proc. ODP, Sci. Res., 145, pp. 195–204.
McManus, J.F., Oppo, D.E., Cullen, J.L., 1999. A 0.5-million-year record of millennial-scale climate variability in the North Atlantic. Science 283, 971–974.
Moore, J.K., Doney, S.C., Glover, D.M., Fung, I.Y., 2002. Iron cycling and nutrient-limitation patterns in surface waters of the World Ocean. Deep Sea Res. 49, 463–507.
Moore, C.M., Mills, M.M., Achterberg, E.P., Geider, R.J., LaRoche, J., Lucas, M.I., McDonagh, E.L., Pan, X., Poulton, A.J., Rijkenberg, M.J.A., Suggett, D.J., Ussher, S.J., Woodward, E.M.S., 2009. Large-scale distribution of Atlantic nitrogen fixation controlled by iron availability. Nat. Geosci. 2. doi:10.1038/ngeo557.
Mullins, C.E., Tite, M.S., 1973. Magnetic viscosity, quadrature susceptibility, and frequency dependence of susceptibility in single-domain assemblies of magnetite and maghemite. J. Geophys. Res. 78, 804–809.
Peck, V.L., Hall, I.R., Zahn, R., Grousset, F., Hemming, S.R., Scourse, J.D., 2007. The relationship of Heinrich events and their European precursors over the past 60 ka BP: multi-proxy ice-rafted debris provenance study in the North East Atlantic. Quat. Sci. Rev. 26, 862–875.
Pettke, T., Halliday, A.N., Hall, C.M., Rea, D.K., 2000. Dust production and deposition in Asia and the north Pacific Ocean over the past 12 Myr. EPSL 178, 397–413.
Prueher, L.M., Rea, D.K., 2001. Volcanic triggering of late Pliocene glaciation: evidence from the flux of volcanic glass and ice-rafted debris to the North Pacific Ocean. Palaeogeogr. Palaeoclimatol. Palaeoecol. 172, 215–230.
Rea, D.K., 1994. The paleoclimatic record provided by eolian deposition in the deep sea: the geologic history of wind. Rev. Geophys. 32, 159–195.
Rea, D.K., Janecek, T.R., 1981. Mass accumulation rate of the non-authigenic inorganic crystalline (eolian) compounds from the western Mid-Pacific Mountains. Init. Repts DSDP, 62. US Govt. Printing Office, Washington, pp. 653–659.
Rea, D.K., Snoeckx, H., Joseph, L.H., 1998. Late Cenozoic eolian deposition in the North Pacific: Asian drying, Tibetan uplift, and cooling of the northern hemisphere. Paleoceanography 13, 215–224.
Rea, D.K., Basov, I.A., Janecek, T.R., Palmer-Julson, A., et al., 1993. Proc. ODP, Init. Repts., 145. Ocean Drilling Program, College Station, TX.
Reynolds, B.C., Aggarwal, J., André, L., Baxter, D., Beucher, C., Brzezinski, M.A., Engstrom, E., Georg, R.B., Land, M., Leng, M.J., Opfergelt, S., Rodushkin, I., Sloane, H.J., van den Boorn, S.H.J.M., Vroon, P.Z., Cardinal, D., 2007. An inter-laboratory calibration of Si isotope reference materials. J. Anal. At. Spectrom. 22, 561–568.
Reynolds, B.C., Frank, M., Halliday, A.N., 2008. Evidence for a major change in silicon cycling in the subarctic North Pacific at 2.73 Ma. Paleoceanography 23 (PA4219). doi:10.1029/2007PA001563.
Robinson, S.G., Maslin, M.A., McCave, I.N., 1995. Magnetic susceptibility variations in Upper Pleistocene deep-sea sediments of the NE Atlantic: implications for ice rafting and paleocirculation at the last glacial maximum. Paleoceanography 10, 221–250.
Schneider-Mor, A., Yam, R., Bianchi, C., Kunz-Pirrung, M., Gersonde, R., Shemesh, A., 2005. Diatom stable isotopes, sea ice presence and sea surface temperature records of the past 640 ka in the Atlantic sector of the Southern Ocean. Geophys. Res. Lett. 32, L10704. doi:10.1029/2005GL022543.
Seki, O., Foster, G.L., Schmidt, D.N., Mackensen, A., Kawamura, K., Pancost, R.D., 2010. Alkenone and boron-based Pliocene pCO_2 records. Earth Planet. Sci. Lett. 292, 201–211.
Shipboard Scientific Party, 1993. Site 882. In: Rea, D.K., Basov, I.A., Janecek, T.R., Palmer-Julson, A. (Eds.), Proc. ODP, Init. Repts, 145, pp. 85–119.
Sigman, D.M., Jaccard, S.L., Haug, G.H., 2004. Polar ocean stratification in a cold climate. Nature 428, 59–63.
Sigman, D.M., Altabet, M.A., François, R., McCorkle, D.C., Gaillard, J.-F., 1999. The isotopic composition of diatom-bound nitrogen in Southern Ocean sediments. Paleoceanography 14, 118–134.
Somes, C.J., Schmittner, A., Altabet, M.A., 2010. Nitrogen isotope simulations show the importance of atmospheric iron deposition for nitrogen fixation across the Pacific Ocean. Geophys. Res. Lett. 37, L23605. doi:10.1029/2010GL044537.
Snoeckx, H., Rea, D.K., Jones, C.E., Ingram, B.L., 1995. Eolian and silica deposition in the central North Pacific: results from sites 885/886. In: Rea, D.K., Basov, I.A., Scholl, D.W., Allan, J.F. (Eds.), Proc. ODP, Sci. Res., 145, pp. 219–230.
Stephenson, A., 1971. Single domain grain distributions I. A method for the determination of single domain grain distributions. Phys. Earth Planet. Inter. 4, 353–360.
Stoner, J.S., Channell, J.E.T., Hillaire-Marcel, C., 1996. The magnetic signature of rapidly deposited detrital layers from the deep Labrador Sea: relationship to North Atlantic-Heinrich Layers. Paleoceanography 11, 309–325.

Sun, D., Bloemendal, J., Rea, D.K., An, Z., Vandenberghe, J., Lu, H., Su, R., Liu, T., 2004. Bimodal grain-size distribution of Chinese loess, and its palaeoclimatic implications. Catena 55, 325–340.

Sun, Y., An, Z., 2005. Late Pliocene–Pleistocene changes in mass accumulation rates of eolian deposits on the central Chinese Loess Plateau. J. Geophys. Res. 110, D23101. doi:10.1029/2005JD006064.

Sun, Y., Liu, Q., 2007. Preliminary comparison of eolian depositions in the North Pacific and the Chinese Loess Plateau during the late Pliocene–early Pleistocene. Quat. Sci. 27, 263–269 (in Chinese with English abstract).

Sun, Y., Clemens, S.C., An, Z., Yu, Z., 2006. Astronomical timescale and palaeoclimatic implication of stacked 3.6-Myr monsoon records from the Chinese Loess Plateau. Quat. Sci. Rev. 25, 33–48.

Swann, G.E.A., 2010. Salinity changes in the North West Pacific Ocean during the late Pliocene/early Quaternary from 2.73 Ma to 2.52 Ma. Earth Planet. Sci. Lett. 297, 332–338.

Swann, G.E.A., Maslin, M.A., Leng, M.J., Sloanne, H.J., Haug, G.H., 2006. Diatom $\delta^{18}O$ evidence for the development of the modern halocline system in the subarctic northwest Pacific at the onset of major Northern Hemisphere glaciation. Paleoceanography 21 (PA1009). doi:10.1029/2005PA001147.

Takeda, S., 1998. Influence of iron availability on nutrient consumption ratio of diatoms in oceanic waters. Nature 393, 774–777.

Thompson, R., Oldfield, F., 1986. Environmental Magnetism, Allen and Unwin, Winchester, Mass.

Tiedemann, R., Haug, G.H., 1995. Astronomical calibration of cycle stratigraphy for Site 882 in the Northwest Pacific. In: Rea, D.K., Basov, I.A., Scholl, D.W., Allan, J.F. (Eds.), Proc. ODP, Sci. Res., 145, pp. 283–292.

Tsuda, A., Takeda, S., Saito, H., et al., 2003. A mesoscale iron enrichment in the western Subarctic Pacific induces a large centric diatom bloom. Science 300, 958–961.

Verosub, K.L., Roberts, A.P., 1995. Environmental magnetism: past, present and future. J. Geophys. Res. 100, 2175–2192.

Watkins, S.J., Maher, B.A., Bigg, G.R., 2007. Ocean circulation at the Last Glacial Maximum: a combined modeling and magnetic proxy-based study. Paleoceanography 22 (PA2204). doi:10.1029/2006PA001281.

Weeks, R., Laj, C., Endignoux, L., Fuller, M., Roberts, A., Manganne, R., Blanchard, E., Goree, W., 1993. Improvements in long-core measurement techniques: applications in palaeomagnetism and palaeoceanography. Geophys. J. Int. 114, 651–662.

Weeks, R.J., Roberts, A.P., Verosub, K.L., Okada, M., Dubuisson, G., 1995. Magnetostratigraphy of Late Cenozoic sediments from ODP Leg 145, North Pacific Ocean. In: Rea, D.K., Basov, I.A., Scholl, D.W., Allan, J.F. (Eds.), Proc. ODP, Sci. Res., 145, pp. 491–521.

Yamazaki, T., Ioka, N., 1997. Environmental rock-magnetism of pelagic clay: implications for Asian eolian input to the North Pacific since the Pliocene. Paleoceanography 12, 111–124.